Performance of Earthquake Early Warning Systems during the 2016–2017 M_w 5–6.5 Central Italy Sequence

by Gaetano Festa, Matteo Picozzi, Alessandro Caruso, Simona Colombelli, Marco Cattaneo, Lauro Chiaraluce, Luca Elia, Claudio Martino, Simone Marzorati, Mariano Supino, and Aldo Zollo

ABSTRACT

Earthquake early warning systems (EEWSs) are nowadays contributing to seismic risk mitigation actions, both in terms of losses and societal resilience, by issuing an alert promptly after the earthquake origin and before the ground-shaking impacts the target to be protected. In this work, we analyze the performance of network-based and stand-alone (on-site) early warning systems during the 2016–2017 central Italy sequence, characterized by events with magnitude as large as 6.5. For the largest magnitude event, both systems predict well the ground shaking nearby the event source, with a rate of success in the 85%–90% range, within the potential earthquake damage zone. However, the lead time, that is, the time available for security actions, is significantly larger for the network-based system. For the regional system, it increases to more than 10 s at 40 km from the event epicenter. The stand-alone system performs better in the near-source region, still showing a positive albeit small lead time (<2 s). Far away from the source (>60 km), the performances slightly degrade, mostly owing to the large uncertainty in the attenuation relationships. This study opens up the possibility for making an operational EEWS in Italy, based on the available acceleration networks, provided that the delay due to data telemetry has to be reduced.

INTRODUCTION

A devastating and long-lasting earthquake sequence shook central Italy between August 2016 and January 2017, generating about 300 causalities and diffuse damage estimated up to 1.4% of Italy GDP and forcing more than 30,000 people to be displaced from their home, as reported on the Italian civil protection website (Chiaraluce *et al.*, 2017). Until now, the sequence generated more than 1000 events with moment magnitude (M_w) larger than 3.0 (National Institute of Geophysics and Volcanology [INGV] catalog; see Data and Resources). It started with the M_w 6.0 Amatrice earthquake occurring on 24 August 2016, without being preceded by a significant foreshock activity. Then, two months later, an M_w 5.9 event (Visso earthquake) nucleated 20 km north of Norcia. These two earthquakes likely contributed to the development of the largest magnitude event (M_w 6.5 Norcia earthquake), which occurred on 30 October 2016. This event ruptured an about 40-km-long fault bridging the seismic gap left from the previous two earthquakes, partially extending over regions already hit by the previous seismicity (Chiaraluce *et al.*, 2017). The last event of the sequence occurred south of Amatrice, on 18 January 2017 (M_w 5.5 Montereale earthquake).

This sequence affected a sector of the central Apennines bounded at north by the 1997 Umbria–Marche sequence and at south by the 2009 L'Aquila earthquake. The ruptures associated with the seismic events almost covered the whole area between the two regions except for a 15–20-km-long segment, north of L'Aquila, that may still represent a seismic gap, thus increasing the potential to generate in this area an $M_w > 5.5$ event in the future. From the aftershock distribution, the sequence occurred along a segmented normal fault system with an along-strike extension of about 70 km (Chiaraluce *et al.*, 2017). The rupture of the main events reached the surface with a significant slip (larger than 30 cm for the Amatrice event and 2 m for the mainshock), along an about 20-km-long trace on the Monte Vettore region (Livio *et al.*, 2016; Emergeo W.G. *et al.*, 2016; Pucci *et al.*, 2017). Kinematic inversions of the main events obtained from geodetic and/or strong-motion data revealed localized slip patches, with maximum slip reaching 1 m for the M_w 6.0 Amatrice event (Tinti *et al.*, 2016; Liu *et al.*, 2017) and about 2 m for the M_w 6.5 Norcia earthquake (Chiaraluce *et al.*, 2017; Liu *et al.*, 2017). The presence of localized slip together with fast rupture propagation enhanced both along-strike and up-dip directivity effects, as it can be recognized in the ground-motion distribution (Liu *et al.*, 2017; Picozzi *et al.*, 2017) and in the pulse-like signature of the near-source waveforms (Iervolino *et al.*, 2016).

For this study, we selected nine events, representing the earthquakes with magnitude larger than 5.0; this threshold yields good signal-to-noise ratio (SNR) at accelerometers within ~100 km from the hypocenters. The list of events is

doi: 10.1785/0220170150

Table 1
Earthquake Parameters for the 2016–2017 Central Italy Dataset (see Data and Resources)

Event Number	M_w	Origin Time (yyyy/mm/dd hh:mm:ss)	Latitude (°N)	Longitude (°E)	Depth (km)	Number of Stations
1	6.0	2016/08/24 01:36:32	42.6983	13.2335	8.1	169
2	5.4	2016/08/24 02:33:29	42.7922	13.1507	8.0	146
3	5.4	2016/10/26 17:10:36	42.8802	13.1275	8.7	172
4	5.9	2016/10/26 19:18:06	42.9087	13.1288	7.5	181
5	6.5	2016/10/30 06:40:18	42.8322	13.1107	9.2	171
6	5.1	2017/01/18 09:25:42	42.5468	13.2623	9.2	138
7	5.5	2017/01/18 10:14:12	42.5293	13.2823	9.1	148
8	5.4	2017/01/18 10:25:26	42.4943	13.3112	8.9	136
9	5.0	2017/01/18 13:33:37	42.4773	13.2807	10	142

reported in Table 1. Although a regional earthquake early warning system (EEWS) was under testing at the INGV during the sequence, we cannot directly analyze the associated real-time performances. Indeed, the current seismic networks in central Italy are not designed to support an early warning (EW), owing to latency in data packeting, to data transmission without controlled delay, and to stations sending data in trigger mode, after the event detection (for sake of comparison, the telemetry at the Irpinia Seismic Network [ISNet] accelerometric network in southern Italy has been specifically designed for real-time data transmission and the associated delay is smaller than 1 s; e.g., Satriano *et al.*, 2011). For this reason, we analyzed the performances by playing backthe waveforms in the EEWS, as they were acquired in real time, with a maximum latency, due to data packeting, of 1 s and no transmission delay, thus corresponding to a nearly optimal situation for evaluating the system performances.

EEWSs are real-time-controlled systems that process the seismic signals radiated by an earthquake rupture while it is still evolving; they predict the ground shaking at selected target sites and they possibly pilot automatic actions aimed at protecting people and machineries, thus facilitating the postevent resilience of struck communities or industrial plants. These systems analyze the early portion of the *P*-wave to forecast the *S*-wave shaking both at near-fault locations and at farther sites. EEWSs are typically classified in two approaches: regional (or network-based) and on-site (or stand-alone) systems. A regional system uses dense strong-motion networks surrounding faults known as potential seismic threats, and it is aimed at detecting, locating, and estimating the size of an earthquake from the analysis of the first few seconds of the *P*-wave record. Then, they predict the expected ground motion at targets through empirical ground-motion prediction equations (GMPEs; Allen and Kanamori, 2003; Zollo *et al.*, 2006). Earthquake size estimation from regional EEWS may saturate when limiting the analysis to a fixed *P*-wave time window (Zollo *et al.*, 2006; Festa *et al.*, 2008). Saturation can be avoided when expanding the *P*-wave time window (Colombelli, Zollo, *et al.*, 2012) or following the growth of the strong-motion data from the *P*-wave onset (Colombelli *et al.*, 2014). A relevant EW parameter is the lead time, that is, the time available for emergency actions after issuing the alert. It depends on the distance between the earthquake source and the site to protect. The lead time is negative for sites located nearby the earthquake epicenter, defining the blind or no warning zone, whose size depends on geometrical (i.e., network density and epicenter-to-target distance) and technological (i.e., telemetry and computational time) parameters. It is as large as 25–30 km for standard dense networks in near-fault observatories (Satriano *et al.*, 2011; Picozzi *et al.*, 2015). Despite this limitation, however, several network-based EEWSs are operational worldwide (e.g., in Romania, United States, Mexico, and Japan). The experimentation of seismic EW in Italy is limited to a pilot testing phase in southern Italy, where the system uses the ISNet (Iannaccone *et al.*, 2010) as the backbone monitoring infrastructure.

On-site systems are based on one or more seismic sensors installed at the site to be protected, where early *P*-wave signals are analyzed to predict the following shaking caused by *S* and surface waves through empirical amplitude-scaling relationships defined at a regional level (Kanamori, 2005; Zollo *et al.*, 2010). Although the estimation of source parameters from stand-alone systems is less robust and accurate than for network-based systems, they usually provide reliable predictions for the peak ground-motion parameters, and they provide a nonnegative lead time for targets located close to the fault. Such systems usually operate in trigger mode, issuing the alert based on predefined thresholds, calibrated on the ground-motion intensity (Wu and Kanamori 2008; Zollo *et al.*, 2010; Colombelli *et al.*, 2015).

In this study, we evaluated the performances of both the network-based PRobabilistic and Evolutionary early warning SysTem (PRESTo) v.1.0 (Satriano *et al.*, 2010) and the stand-alone on-Site-Alert-leVEl (SAVE) v.1.0 (Caruso *et al.*, 2017) EEWS on the main events of the central Italy sequence. In the Data and Methods section, we describe the selected dataset in terms of events and stations and summarize the primary features of the two systems. Then, we discuss the performances of the two EEWSs, both for the M_w 6.5 Norcia earthquake and considering all the selected events. The performance analysis is based on the correct estimation of the strong-motion parameters and on the available lead time as a function of the distance

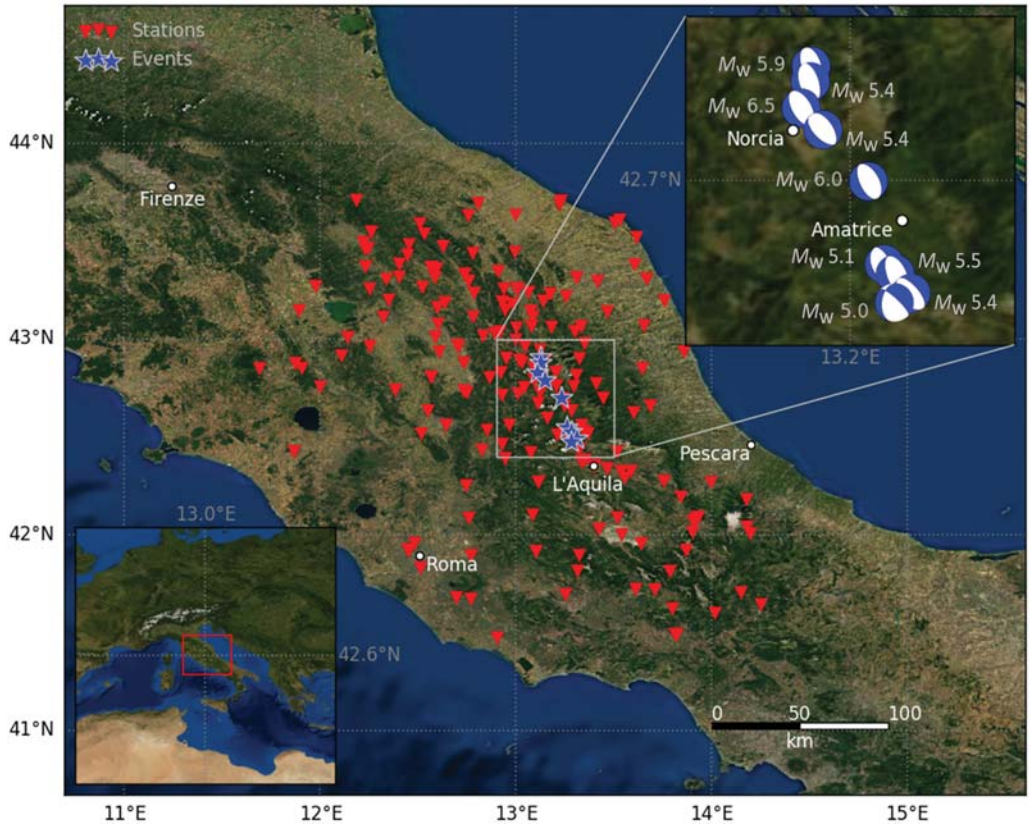

▲ **Figure 1.** Map of the accelerometric stations from Civil Protection Department and National Institute of Geophysics and Volcanology (INGV, red triangles) and earthquakes of the 2016–2017 central Apennines sequence with $M_w \geq 5$ considered in this study (blue stars). In the upper inset, details about earthquake location, focal mechanism, and moment magnitude are shown (data from INGV network, Engineering Strong Motion database; see Data and Resources).

from the earthquake epicenters. In the case of the network-based system, we also compare the location and the magnitude estimated by the EEWS with the reference values.

DATA AND METHODS

The dataset considered in this study consists of nine earthquakes with M_w larger than 5.0, occurred in the central Italy region from 24 August 2016 to 18 January 2017 and recorded by ~200 accelerometric stations located at epicentral distances in the 10–130 km range. The acceleration records were retrieved from the Engineering Strong Motion database (Luzi *et al.*, 2016), which freely distributes strong-motion data from earthquakes that have occurred in the European–Mediterranean and the Middle East regions.

For each event, we selected unprocessed acceleration waveforms from all the available stations in the selected distance range. The stations belong to the Italian Strong Motion Network (Rete Accelerometrica Nazionale [RAN]), operated by the Italian Department of Civil Protection, and to the Italian National Seismic Network, operated by the INGV. The list of events with the associated source parameters and the number of stations that recorded these events is reported in Table 1. In Figure 1, the areal distribution of events and stations is shown. In the epicentral area, the station coverage is very dense, with an average interstation distance of about 10 km.

Network-Based EEWS

We used PRESTo as the network-based EEWS to evaluate the performances. PRESTo is a free and open-source platform (see Data and Resources; Iannaccone *et al.*, 2010; Satriano *et al.*, 2011). The system processes in real time the continuous accelerometric data streams from a seismic network and, after the event detection, it promptly provides probabilistic and evolutionary estimates of location and magnitude, as well as the ground-shaking prediction at target sites through GMPEs. Furthermore, during an event, PRESTo v.1.0 delivers messages to target sites containing all relevant earthquake parameters before the arrival of destructive waves, to enable automatic safety procedures, accomplishing the goal of an EEWS.

PRESTo v.1.0 implements the following components: (1) the phase detector and picker algorithm Filter Picker (Lomax *et al.*, 2012), which picks the *P*-wave first arrival; it is optimized for real-time seismic monitoring and EW; (2) the location algorithm RTLoc (Satriano *et al.*, 2008), which locates earthquakes exploiting both triggered and not-yet-triggered stations; it provides a fully probabilistic description of the hypocenter coordinates and origin time; (3) the algo-

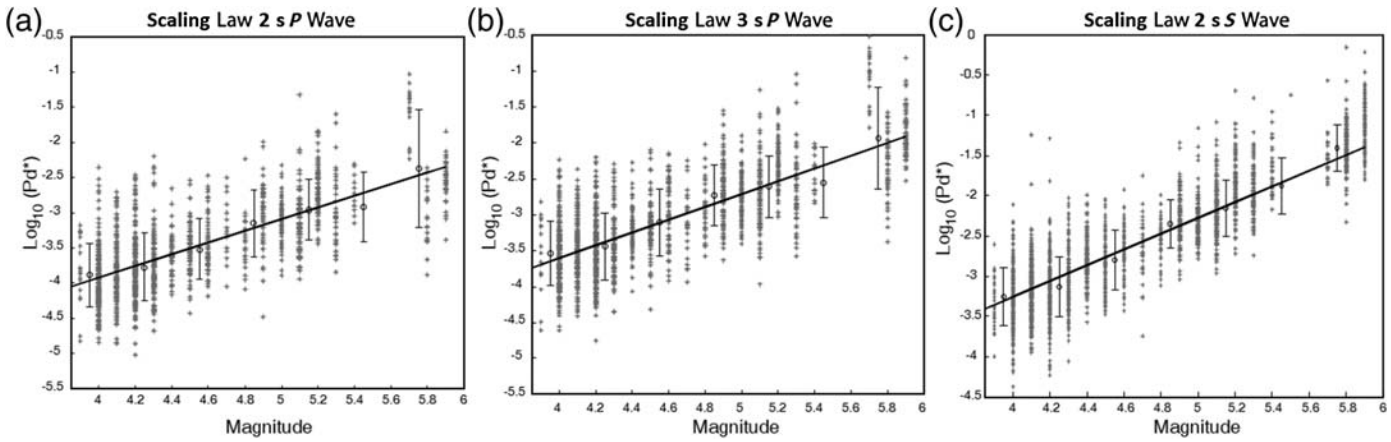

▲ **Figure 2.** Scaling relationships between the peak displacement measured on (a) 2 s and (b) 3 s of *P* wave and (c) 2 s of *S* wave and the final event magnitude. To compare all data in the same plot, the peak displacement values have been computed to the reference distance of 10 km and they are referred in the graphs to as Pd*.

rithm for estimating the magnitude RTMag (Lancieri and Zollo, 2008), which is based on a Bayesian approach and uses the peak displacement measured on the first seconds (2 and 3 s of *P* wave and 2 s of *S* wave) of the high-pass-filtered signal, with a cutoff frequency of 0.075 Hz; the final earthquake magnitude is obtained through empirical correlation laws based on early *P* and *S* peak displacement values; and (4) GMPEs for estimating the peak ground motion (i.e., peak ground velocity [PGV] and peak ground acceleration) at target sites and at seismic stations using the real-time evolutionary estimates of location and magnitude.

PRESTo v.1.0 is currently running in real time, collecting and analyzing data from ISNet since 2009 (Iannaccone *et al.*, 2010). Real-time testing is also underway in South Korea on the Korean Institute for Geoscience and Mineral Resources (KIGAM) network, in Romania on the Romanian Seismic Network (RoNet; National Institute of Research and Development for Earth Physics), in the Marmara region (Turkey) on the Kandilli Observatory and Earthquake Research Institute (KOERI) network, and in a transnational region including northeast Italy, Slovenia, and Austria at the Istituto Nazionale di Oceanografia e Geofisica Sperimentale center. The calibration of the empirical laws between peak displacement and earthquake magnitude (M_w) used in this study has been carried out using a dataset of about 5000 accelerometric records from the RAN related to the largest earthquakes ($M_w > 4$) that occurred in Italy during the period 1997–2013 and available through the ITalian ACcelerometric Archive 2.0 (Pacor *et al.*, 2011; see Data and Resources). The dataset includes recordings that span hypocentral distances from 10 to 300 km, and magnitudes M_w from 4.0 to 6.3, with most of the hypocentral distances smaller than 60 km. Furthermore, the dataset includes the mainshock and the largest aftershocks of the M_w 6.3 L'Aquila and the M_w 5.9 Emilia earthquakes, which occurred in April 2009 and May 2012, respectively. The results of the best-fit regression analysis for the *P* waves (i.e., 2 and 3 s) and *S* waves (i.e., 2 s) windows are as follows:

$$2\ \mathrm{s}(P_{\mathrm{wave}}):\ \log(\mathrm{Pd}_P) = -7.26(\pm 0.90) + 0.83(\pm 0.18)M_w - 1.57(\pm 0.05)\log(r/10);\quad \sigma = 0.51;\ R^2 = 0.96$$

$$3\ \mathrm{s}(P_{\mathrm{wave}}):\ \log(\mathrm{Pd}_P) = -7.17(\pm 0.83) + 0.89(\pm 0.17)M_w - 1.91(\pm 0.05)\log(r/10);\quad \sigma = 0.47;\ R^2 = 0.96$$

$$2\ \mathrm{s}(S_{\mathrm{wave}}):\ \log(\mathrm{Pd}_S) = -7.18(\pm 0.55) + 0.98(\pm 0.12)M_w - 1.19(\pm 0.03)\log(r/10);\quad \sigma = 0.36;\ R^2 = 0.98,$$

in which r is the hypocentral distance in kilometers, Pd_P and Pd_S are measured in meters, σ is the standard deviation on the $\log(\mathrm{Pd}_X)$ estimate, and R is the correlation coefficient. In Figure 2, we show the best-fit curves superimposed to the data; to compare observations collected at different hypocentral distances, the peak displacement is reduced to an equivalent distance of 10 km, according to the above relationships. Figure 2a, 2b, and 2c corresponds to the best-fit solutions for 2 and 3 s of *P* wave and 2 s of *S* wave, respectively.

Finally, the GMPEs are derived from strong-motion records of 131 earthquakes that occurred in Europe and in the Middle East with moment magnitudes ranging from M_w 5 to 7 (Akkar and Bommer, 2007).

Stand-Alone EEWS

SAVE v.1.0 (Caruso *et al.*, 2017) is used as the stand-alone EEWS for this analysis. It is a *P*-wave-based EEWS that measures in real time the peak displacement (Pd) and the predominant period (τ_c) over time windows of variable length (i.e., 1, 2, and 3 s) after the *P*-phase arrival (Wu and Kanamori, 2008). Thus, it provides the expected ground-shaking intensity at the monitored site, a local alert level (Colombelli, Amoroso, *et al.*,

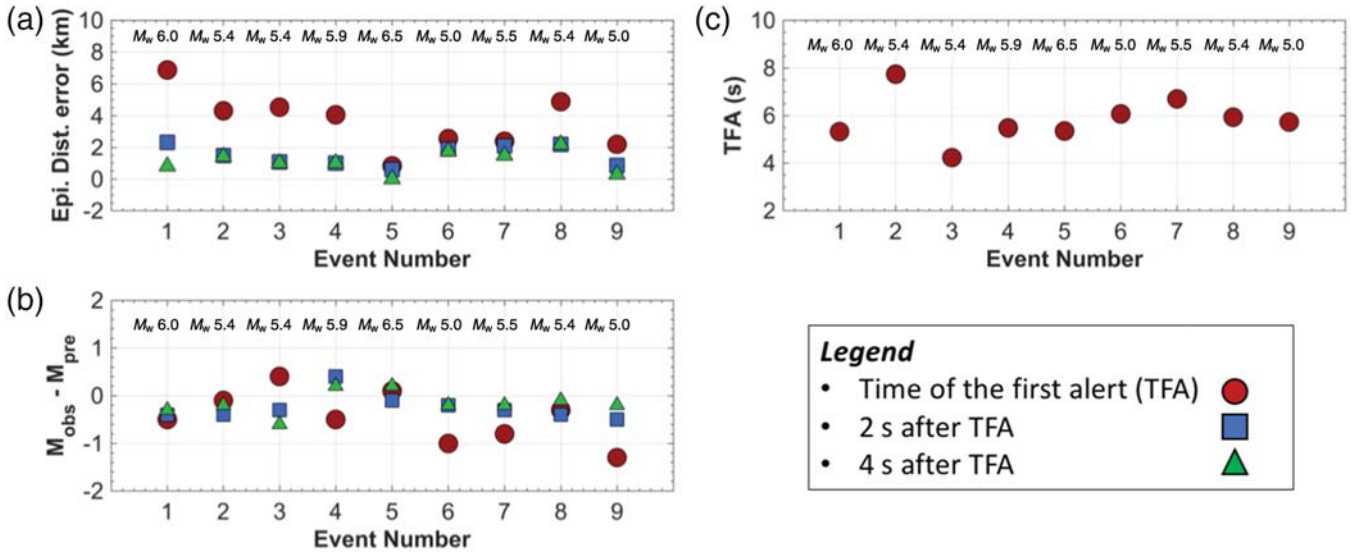

▲ **Figure 3.** (a) Epicentral location error at the time of the first alert (TFA), 2 and 4 s after the TFA. (b) Residuals between observed and predicted magnitude at TFA, 2 and 4 s plus TFA. The error for both location and magnitude is computed as the difference between the estimations provided by PRobabilistic and Evolutionary early warning SysTem (PRESTo) v.1.0 and the values given by the official INGV bulletin. (c) TFA in seconds. This value ranges between 4 and 8 s, with an average value of 6 s.

2012), and a qualitative classification of the earthquake magnitude and of the source–receiver distance. SAVE v.1.0 can operate either at a single station (i.e., a single sensor located at the target site) or with a small set of collocated seismic nodes. Independently of the number of sensors acquired by SAVE v.1.0, the algorithm checks the quality of detected picks and measures the EW parameters Pd and τ_c only if some criteria are fulfilled. Specifically, we require that the SNR, defined as $\mathrm{SNR} = 20\log_{10}(\mathrm{Pd}/\mathrm{PGD}_{\mathrm{noise}})$, is $\mathrm{SNR} > 14$, the following relationship $-0.9 < \log_{10}(\mathrm{Pv}/\mathrm{Pd}) < -0.2$ holds and the data are not clipped (Caruso *et al.*, 2017). In the formulas, $\mathrm{PGD}_{\mathrm{noise}}$ is the peak displacement measured in a 3 s time window before the arrival of the *P* wave and, Pd and Pv are peak displacement and velocity, respectively, recursively measured in time windows of 1, 2, and 3 s after the *P* pick. These conditions ensure that residual baselines in the displacement do not significantly affect the measure of the EW parameters.

The empirical scaling relationships between Pd, τ_c, PGV, M_w, and *R* used by SAVE v.1.0 also have been calibrated on the Italian RAN dataset (Caruso *et al.*, 2017). Similar to PRESTo v.1.0, SAVE v.1.0 delivers alert messages via the Internet whenever a detected event exceeds user-configurable thresholds of the output parameters (e.g., estimated intensity equal to VI or above). The warning message includes the EW parameters calculated by SAVE v.1.0 and their uncertainties. A new message is sent at each change of outputs or whenever a second has passed from the previous message.

RESULTS

Performance of the Network-Based EEWS

We investigated the performances of the regional EEWS by injecting in playback mode the waveforms related to the central Italy earthquakes in PRESTo v.1.0. Results of the analysis are shown in Figure 3. The performance of the system is assessed in terms of its capability to correctly provide the location, the magnitude, and the time of the first alert (TFA), this latter being defined as the instant from the event origin time when five stations have triggered and the PRESTo v.1.0 provided the first estimate of location and magnitude. The error associated with the EW estimates is considered as the difference between the results obtained by PRESTo v.1.0 and those provided by the official INGV bulletin (see Data and Resources). Furthermore, to investigate the stability of the EW estimates, we consider the estimations at TFA, and at this latter quantity plus 2 and 4 s.

Figure 3a and Table 2 show that the error in epicentral location at TFA ranges between 0.8 and 6.9 km, these values being obtained for the M_w 6.5 Norcia and the M_w 6.0 Amatrice earthquakes, respectively. The location error does not show any trend with magnitude and depth (i.e., differences in hypocentral depth among the events are within 2.5 km), suggesting that the observed errors are due to an inherent aleatory variability in the arrival time of the *P* wave at the closest stations. The number of stations for which arrival times were available at TFA varies between 5 and 15 (Table 2). Two seconds after the TFA, the epicentral errors are already very small (i.e., below 2.5 km and on average of about 1.5 km), and they remain almost constant when extending the time to 4 s after the first alert (Table 3). The number of stations included in the analysis 2 s after the TFA ranges between 14 and 30.

Figure 3b presents the results in terms of event magnitude. At the TFA, the magnitude tends, in general, to overestimate the reference values with an average difference of 0.4 magnitude units (mu). Specifically, the largest overestimations are obtained for two M_w 5.0 events (events 6 and 9 with +0.8 and +1.3 mu, respectively). These events show errors in hypocen-

Table 2
PRESTo v.1.0 Performance at the Time of the First Alert (TFA)

Event Number	M_w	Number of Triggered Stations	Δ Time after Origin Time (s)	Blind Zone (km)	Δ Epicentral Location (km)	Magnitude by PRESTo
1	6.0	7	5.3	17.4900	6.9	6.5
2	5.4	5	7.7	25.4100	4.3	5.5
3	5.4	7	4.2	13.8600	4.5	5.0
4	5.9	11	5.5	18.1500	4.0	6.4
5	6.5	15	5.4	17.8200	0.8	6.4
6	5.1	13	6.1	20.1300	2.6	6.1
7	5.5	13	6.7	22.1100	2.4	6.3
8	5.4	5	5.9	19.4700	4.9	5.7
9	5.0	15	5.7	18.8100	2.2	6.3

The symbol Δ represents the absolute value of the difference between the estimation of PRESTo and the bulletin reference values. PRESTo, PRobabilistic and Evolutionary early warning SysTem.

Table 3
PRESTo Performance at the Time of the First Alert (TFA) Plus 2 and 4 s

Event Number	M_w	Δ Epic. TFA + 2 s (km)	Δ Epic. TFA + 4 s (km)	M_w by PRESTo TFA + 2 s	M_w by PRESTo TFA + 4 s
1	6.0	2.3	0.8	6.4	6.3
2	5.4	1.5	1.4	5.8	5.6
3	5.4	1.1	1.0	5.7	6.0
4	5.9	1.0	1.0	5.5	5.7
5	6.5	0.6	0.0	6.6	6.3
6	5.1	1.9	1.7	5.3	5.3
7	5.5	2.1	1.5	5.8	5.7
8	5.4	2.2	2.2	5.8	5.5
9	5.0	0.8	0.3	5.5	5.2

The symbol Δ represents the absolute value of the difference between the estimation of PRESTo and the bulletin reference values.

tral location below 3 km. Therefore, we believe that the anomalous magnitude overestimations could be originated either by the *S*-wave contamination in the selected *P*-wave time window at the closest stations and/or by source effects, such as the radiation of large initial *P*-peak amplitudes generated by relatively high fault slip or stress release in the regions of the fault located nearby the nucleation area. The aftershocks of this seismic sequence presented a quite large variability in the dynamic properties (Picozzi *et al.*, 2017; i.e., apparent stress between 1 and 20 MPa). Large apparent stress (i.e., large rupture speed, large static stress drop, and large slip) might have led to 2 s *P*-wave displacement amplitudes anomalously larger with respect to those expected from the empirical relationships calibrated for Italy. Concerning the three largest events of the sequence, in the case of the M_w 6.0 Amatrice and M_w 5.9 Visso earthquakes, the EW estimates are 0.5 mu larger than the final magnitude, while in the case of the M_w 6.5 Norcia earthquake, the EW estimate agrees very well with the final value, with a difference of −0.1 mu. Two seconds later, the number of stations contributing to the magnitude estimate is greater than 10, and we generally observed an error reduction of 0.2 mu on average (Table 3). At this stage, stations closer to the epicenter contributed with the *S* wave, whereas farther stations provided 2 or 3 s of *P* wave for the magnitude estimate. Finally, 4 s after TFA, the error associated with the magnitude decreases to 0.1 mu (Table 3).

The TFA varies from 4.2 s (i.e., event 3) to 7.7 s (i.e., event 2), with an average value of 5.8 s (Fig. 3c). These values can be used to estimate the radius of the blind zone (BZ) assuming for the *S* wave a constant velocity of 3.3 km/s, which leads to BZs' radii between 14 and 25 km (19 km in average). These estimates are consistent with the results of Picozzi *et al.* (2015), who evaluated the BZ radius based on numerical simulations. Although the computation time is considered in the playbacks, it is here assumed that no latency is due to data telemetry, while a maximum of 1 s of delay is ascribed to data

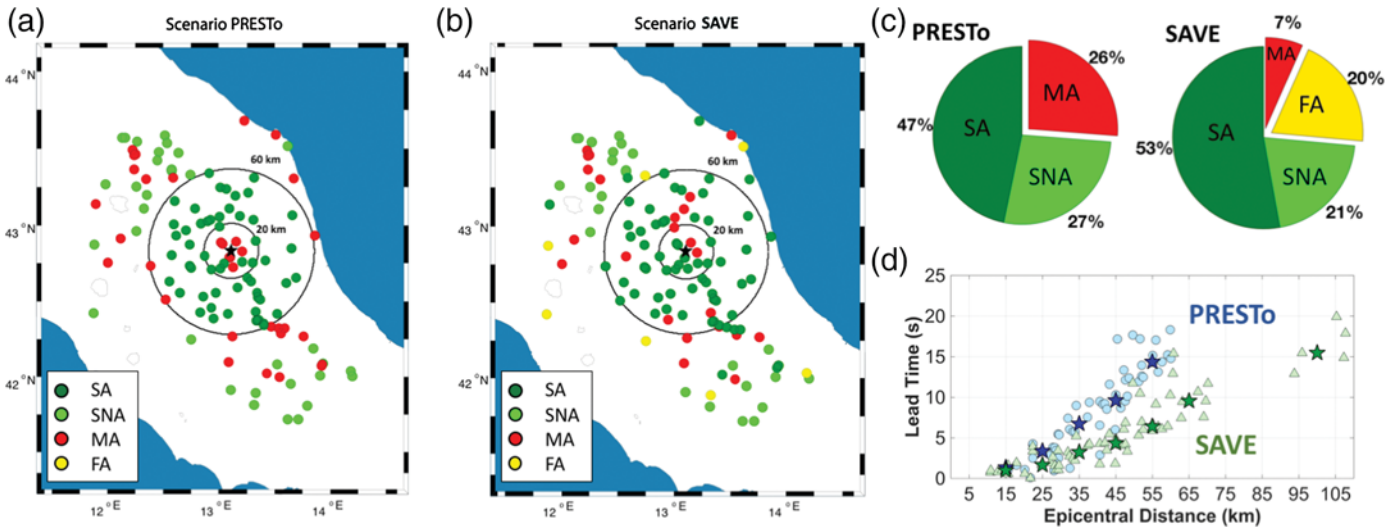

▲ **Figure 4.** Performances of the network-based (PRESTo v.1.0) and stand-alone (on-Site-Alert-leVEl [SAVE] v.1.0) earthquake early warning system (EEWS) for the M_w 6.5 Norcia earthquake. (a) Areal distribution of successful alerts (SA), successful no-alerts (SNA), missed alerts (MA), and false alerts (FA) by PRESTo v.1.0. Circles enclose stations within 20 and 60 km. (b) Areal distribution of SA, SNA, MA, and FA using SAVE v.1.0. (c) Pie charts illustrating the percentage of SA, SNA, MA, and FA for the two systems. (d) Lead time as a function of the distance for PRESTo v.1.0 (blue circles) and SAVE v.1.0 (green triangles). Stars indicate the median value for 10-km-wide distance bins.

packeting. Therefore, the derived values represent the lower bound for the BZ size. They are, however, useful estimates for guidance in assessing the performance of the EEWS given by the integration of PRESTo v.1.0 on the Italian seismic network. In real-time data acquisition mode, the BZ dimension would progressively increase with the increase of delay in data telemetry.

Furthermore, we also evaluated the capability of the system to provide reliable alerts at sites located at an increasing distance from the epicenter. From the user point of view, indeed, an EEWS should provide information about the incoming ground shaking, the possible overcoming of a damage threshold for the buildings, and how much lead time is available to secure people, structures, and industrial machineries against the potential earthquake damage.

To set the ground-motion level of interest, we considered the PGV corresponding to the lower bound of the macroseismic intensity degree VI in the Mercalli–Cancani–Sieberg (MCS) scale (Sieberg, 1930) (light damage and strong perceived shaking), and we exploited the relationships between PGV and MCS intensity recently calibrated for Italy (Faenza and Michelini, 2010) (lower bound of intensity VI corresponds to a PGV of 2.4 cm/s). For each event, we assumed all the available accelerometric stations within 200 km from the epicenter as potential target sites, and we compared the observed PGV with the PGV predicted by PRESTo v.1.0 at TFA (i.e., on the base of the first location and magnitude estimates and using the selected GMPE). An alert is considered a successful alert (SA) when both observed and predicted PGV values are larger than the threshold; we get a successful no-alert (SNA) when both values are below the selected threshold, a false alarm (FA) when the predicted PGV is above while the observed PGV is below the threshold, and finally, a missed alarm (MA) when the observed PGV is above the threshold but not the predicted PGV. It is worth noting that during the playback of all the records, PRESTo v.1.0 never missed the real-time detection of the events. Therefore, the users outside the BZ would have never experienced a missed event detection but eventually an underestimated prediction of the ground-motion severity. Similarly, the meaning of false alert is only caused by an overestimation of the ground shaking. Additionally, because our real-time location and magnitude estimates are consistent with those provided by the INGV bulletin, the performance of the regional EEWS is critically influenced by the prediction capability of the GMPEs.

Concerning the lead time, we computed it as the difference between the instant at which the ground velocity overcomes for the first time the threshold value of 2.4 cm/s and the TFA. It is worth noting that this definition of the lead time is related to the effective arrival of the ground shaking of interest for the EEWS; a more conservative definition, which is also used by other EEWS, is based on the theoretical arrival time of the *S* wave at the target site. Figure 4a shows the performance of PRESTo v.1.0 for the M_w 6.5 Norcia earthquake at TFA using 122 stations with a maximum epicentral distance of 130 km. At this time, four stations with an epicentral distance smaller than 13 km were already hit by a PGV larger than 2.4 cm/s and were thus classified as missed alerts. Between 13 and 16 km, two stations were successfully alerted and two were missed. Beyond 16 km and up to 60 km, where the instrumental intensities estimated by the INGV were between VI and IX (see Data and Resources), all the stations (i.e., 55) received a successful alert. Therefore, in the area experiencing a severe ground motion, the EEWS rated 90.5% of successful alerts

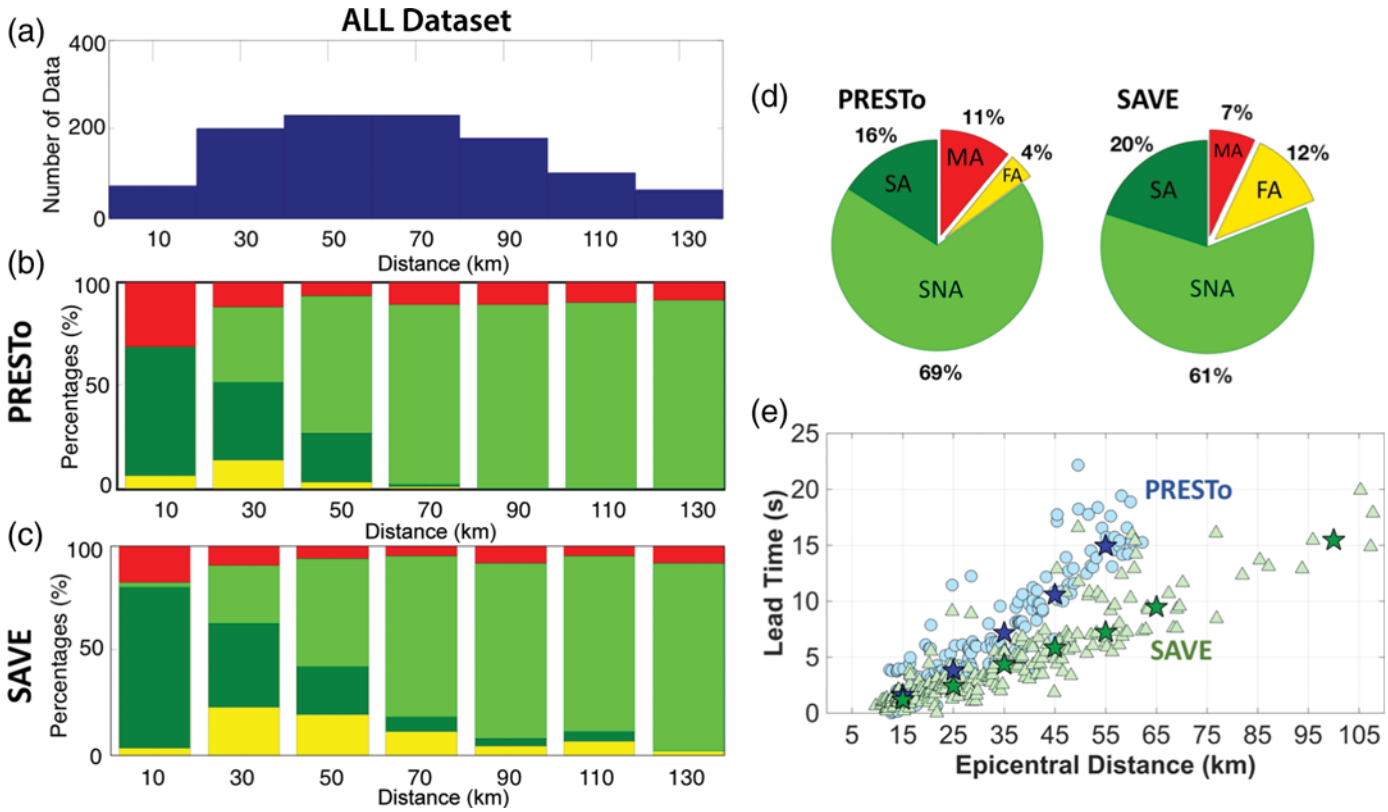

▲ **Figure 5.** Overall performances of the network-based (PRESTo v.1.0) and the stand-alone (SAVE v.1.0) EEWS. (a) Histogram of the number of available stations as a function of the distance; (b) rate of SA, SNA, MA, and FA using PRESTo v.1.0 as a function of the distance. (c) Rate of SA, SNA, MA, and FA using SAVE v.1.0 as a function of the distance. (d) Pie charts illustrating the percentage of SA, SNA, MA, and FA for the two systems. (e) Lead time as a function of the distance for PRESTo v.1.0 (blue circles) and SAVE v.1.0 (green triangles). Stars indicate the median value for different distance bins.

and 9.5% of missed alerts, the latter percentage representing the stations within the BZ. Then, for larger epicentral distances (i.e., between about 60 and 134 km), 33 stations were correctly alerted and classified as SNA, whereas 32 stations resulted as MA. For this external area, where the instrumental intensity was estimated between V and VI, almost 50% of the MA can be likely attributed to local site conditions which have led to small fluctuations of the observed PGV, or to large amplitude surface waves, in both cases resulting in jumps between intensity V and VI with respect to the intensities predicted by the GMPEs. A confirmation of our observations comes also from the macroseismic survey of the epicentral area (Arcoraci *et al.*, 2016), which is not based on the PGV and shows intensities equal or larger than VI limited to about 40 km from the epicenter. Therefore, our performance rule is probably strongly conservative, by assigning MA at large epicentral distances (i.e., beyond 60 km) if we consider that damages were not observed at villages nearby these stations. Globally, the performance of the system is: 47% of SA, 27% of SNA, and 26% MA, with a total rate of success of 74% (i.e., SA plus SNA; Fig. 4c).

Figure 4d shows the lead time computed for the stations with a predicted PGV larger than the selected threshold. We observe that within 20 km from the epicenter the lead time is very short (< 1 s). However, beyond 20 km it rapidly increases to values that would allow trained users to duck and cover: the mean lead-time ranges from 3.5 s between 20 and 30 km to 14.5 s between 50 and 60 km. If we had computed the lead time as the difference between the theoretical arrival time of the *S*-wave arrival time and the TFA, we would have obtained a decrease of the lead time of about 1 s at 45 km and 2 s at 60 km.

When the performance of PRESTo v.1.0 is evaluated over all the selected events, the number of tested station–event pairs raises to 1070, with about 70 pairs within 20 km from the epicenter and an average of about 200 pairs for all the other 20 km wide bins up to 80 km from the epicenter (Fig. 5a). The number of SA decreases with the epicentral distance (i.e., from about 62% between 0 and 20 km to about 22% between 40 and 60 km; Fig. 5b), but the difference is mainly compensated by the number of SNA. Considering SA plus SNA, the correct alerts oscillate between 74% in the 20–40 km range and 88% in the 80–100 km range.

Concerning the false and missed ground-motion predictions, we observe that most of the false detections occur between 30 and 50 km from the epicenter, with a rate of 13%. Instead, the largest portion of MA is concentrated within the 20 km from the epicenter (i.e., 32%), while it decreases to about 12% up to 140 km. The global performance as shown in Figure 5d confirms these results, with correct alerts (i.e., SA

plus SNA) in the 85% of cases, 11% of MA, and 4% of FA. Again, outside the BZ, most of FA and MA owe to the large uncertainty in the GMPEs. Similarly to the Norcia event, the median value of the available lead time (Fig. 5d) is about 3.5 s at 25 km, 7 s at 35 km, 10 s at 45 km, and more than 15 s above 55 km.

Performance of the Stand-Alone EEWS

The performance of the stand-alone EEWS was evaluated by running the software SAVE v.1.0 on the same strong-motion dataset used for the regional analysis. The performance is assessed through the capability of the system to correctly predict the expected ground motion at the sites to be secured. To be directly comparable with the results from the network-based system, we assume that the EEWS issues an alert when the predicted PGV > 2.4 cm/s. Then, we compared the predicted intensity with the observed one and used the same four classes as defined before (SA, SNA, MA, and FA) to assess the performances. Playing back the strong-motion data, SAVE v.1.0 also recognized all the events in the database; again, the notion of false and missed alerts is thus associated with a wrong estimation of the strong-motion severity.

Figure 4b shows the performance of the on-site system for the M_w 6.5 Norcia earthquake. Results are represented in a map to be directly comparable with the outcomes of the regional system, although predictions of the on-site system are evaluated independently station by station. Up to 60 km, almost all stations received an SA, except for two stations located within 15 km from the epicenter, where the ground velocity overcomes the threshold (2.4 cm/s) before issuing the alert, and for four stations located northward of the epicenter, along the fault strike direction. These stations might have experienced possible source effects, likely due to focal mechanism and directivity, or near-field dominated waveforms, which produced a deviation from the average Pd–PGV scaling. Our hypothesis is corroborated by the macroseismic survey (Arcoraci *et al.*, 2016), which provided higher damage levels for villages distributed along-strike direction than for villages in other directions.

Close to the isoseismal VI curve, several targets experienced both MA and FA, with a difference of one unit between the predicted and observed intensities. Most of these results can be attributed to fluctuations related to the discretized intensity scale and to site and source effects around the PGV threshold value of 2.4 cm/s. The final performance of the on-site system is 53% of SA, 21% of SNA, 20% of MA, and 6% of FA. Comparing the percentage of SA and SNA, the performance of the stand-alone system is comparable with that of the regional system.

In Figure 4d, the lead time for the stand-alone system is superimposed to the lead-time estimation for the network-based system for the M_w 6.5 Norcia earthquake. A positive lead time is still available for the closest stations within the first 20 km, albeit very short (< 2 s). Then, its median value increases from about 2 s between 20 and 30 km to about 7 s between 50 and 60 km. The overall values of the lead time for an on-site system are smaller than the ones for the regional system, the former growing with the difference between the *S*- and *P*-wave slowness, the latter increasing with *S*-wave slowness.

Figure 5c finally summarizes the performances for all the events in the sequence. Within 30 km from the epicenter, the system reported the 77% of SA/SNA. The larger portion of MA (i.e., 11%) is concentrated within 20 km from the epicenter, whereas most of FA (i.e., 20%) occurs between 20 and 60 km. The statistics over the entire range of distances confirms the high rate of SA/SNA (i.e., 81%), whereas MA and FA rates are 7% and 12%, respectively (Fig. 5d). The lead time increases from few seconds (< 2 s) in the near-source range (< 15 km), to 4 s at 35 km, and above 7 s beyond 55 km (Fig. 5e).

DISCUSSION

The offline application of stand-alone and network-based EEWS to the central Italy sequence enhanced several strong points related to the usability and robustness of earthquake EW in Italy; however, this analysis does not include latency due to data telemetry. The high density of the accelerometric network in the epicentral area enabled the rapid event detection and characterization with regional alerts issued 4–8 s after the event origin time. This corresponds to a BZ with a radius of 15–25 km centered at the epicenter. Outside the BZ, the network-based system predicts well the impending ground shaking by assessing the potential damage area with a rate of success around 90%. While the earthquake location and magnitude are accurately estimated by analyzing the early portion of the *P* wave at the stations close to the epicenter, differences between predicted and observed intensities and PGV mainly owe to the uncertainty in the GMPEs. Although the epistemic variability was already reduced using GMPEs calibrated for this specific area, further improvement can come from accounting for specific source and site effects.

The stand-alone system can provide event information within a still positive lead time in the BZ of the network-based system, although the available time is very short (< 2 s). Within this region, triggering security actions becomes challenging. The overall performance of the on-site system is slightly worse than that of the regional system (rate of success at about 80%). When looking at the alert maps of the Norcia earthquake (Fig. 4a,b), both systems correctly predict the expected ground-shaking intensity within 60 km from the epicenter, and the two maps also almost superimpose far away from the event epicenter. Stand-alone systems show a large rate of false alerts, while reducing the number of missed alerts at large distances from the source. At large distances, the PGV is associated with the arrival of surface waves, which are not taken into account by the adopted GMPEs, while their amplitude can be partially captured by analyzing the early evolution of the *P* wave at the same site.

Although both systems provide equivalent results in terms of rate of success of predicting the ground-shaking intensity, the lead-time distribution shows significant differences and

it increases faster for the network-based system, ranging from 5 to 15 s between 30 and 55 km from the event epicenter. The lead time almost halves for the on-site system in the same distance range, making the latter system less effective on average for this area. Considering the potential social benefit of an EEWS, it is worth noting that, taking into consideration the ring between 30 and 55 km from the epicenter, 5–15 s of available lead time could have been utilized for implementing seismic risk and exposure mitigation actions in 168 municipalities affecting about 700,000 inhabitants. The beneficial effects of an EEWS in this area are even more evident if we consider that the potential end users experienced a six-month-long seismic sequence.

Improvement of site models can reduce epistemic variability in the ground-shaking prediction of regional systems, accounting for velocity, attenuation, and nonlinear rheology in the shallow layers beneath the station, and offsets in the ground-motion parameters at the site with respect to the selected GMPEs (e.g., Abrahamson and Bommer, 2005). Although site effects are intrinsically accounted for in the on-site systems, local discrepancies at specific sites need to be further investigated because the site response to the *P* wave could not linearly change with the response to the *S* wave.

The real-time evaluation of source parameters such as fault geometry, size, directivity, and focal mechanism requires the development of new methodologies, for the evolutionary inversion of the extended source properties. Some techniques were already proposed to improve the source description while the earthquake is still ongoing (Yamada and Heaton, 2008; Böse *et al.*, 2012; Colombelli *et al.*, 2013). Stand-alone systems account for some of the source parameters, such as reduced Joyner–Boore distance due to rupture finiteness. They also track the source directivity through the *P* wave, although it is less enhanced than for *S* wave, because it depends on the ratio between the earthquake rupture and the propagation wave velocities. Finally, the effect of the focal mechanism is not accounted for in the on-site systems, because at the same site larger *P*-wave amplitudes are not always followed by larger *S*-wave amplitudes. In this specific case, the M_w 6.5 Norcia event grew along a 40-km-wide normal fault, with significant slip release in the hypocentral area (a concentrated asperity with slip larger than 2 m), a pretty fast rupture moving to the surface (rupture speed of 2.7 km/s) and large coseismic slip at the surface (Chiaraluce *et al.*, 2017). These features can be the source of some missed alerts in the near-source domain, especially in the footwall of the fault.

A complementary data-driven approach for EEWS to improve ground-shaking prediction is to integrate on-site and regional EEWS in real time to produce an evolutionary ground-shaking map. Such a system should initially combine GMPE-based regional estimates of ground-motion parameters with on-site predictions to define the areal distribution of the ground-motion severity. Then, the maps should be continuously updated as the effective ground motion starts to be collected at the stations close to the epicenter. Integration of network-based and stand-alone systems started to be developed through the definition of the potential damage zone (Colombelli, Amoroso, *et al.*, 2012) and the software QUAKEUP (Zollo *et al.*, 2017), although several issues remain open, such as the separation of *P*- and *S*-wave contributions in the data.

Finally, all results presented here do not account for the delays due to the actual dataloggers and telemetry currently deployed in the seismic networks. Since July 2015, PRESTo v.1.0 is running at the Near Fault Observatory TABOO, located above the Alto Tiberina fault, about 60 km north of the region interested by the sequence. This experimentation was promoted in the framework of the European Plate Observing System - Implementation Phase (EPOS-IP) project. In a parallel installation, PRESTo v.1.0 also run on a part of the INGV national network located in the central Italy, whose data are streamed in real time to the control center of Ancona. For this system, an event is declared if six picks occur within 3 s. The system also worked during the initial part of the sequence, before the M_w 6.5 Norcia earthquake. It provided an alert during the Amatrice earthquake 11.4 s after the first *P* pick and 14.3 s after the origin time. The first estimated location was very close to the one released by the INGV bulletin (error in the epicentral location <2 km), while the magnitude was underestimated by 0.2 mu, the system provided an initial M_w 5.8. The final estimation from PRESTo v.1.0 was instead M_w 6.1. The large delay in the alert was due to the latency in data packeting (2–3 s), in the data transmission (up to 20 s for some stations connected to the control center via satellite), and in the data quality (signal clipping).

Diverse results were obtained for the two 26 October 2016 Visso earthquakes. For the M_w 5.4 event, location and magnitude were close to the reference values from bulletin ones, providing the first alert 6.3 s after the initial *P* pick, and thus 9.0 s after the origin time. For the M_w 5.9 event, alert release was comparable with the previous event, but the magnitude was largely underestimated at the TFA. This was mainly due to the clipping of velocimeter sensors near the epicenter and to the underestimation of the hypocentral depth, which prevented the system from using larger *P*-wave windows due to a supposed *S*-wave contamination. The biased magnitudes required several seconds to be partially balanced by the information coming from the rest of the network. On the other hand, the use of velocimeters was justified in the testing phase needing as much station density as possible because the initial plan was to process smaller size earthquakes during the experimentation at the near-fault observatory.

CONCLUSIONS

In this study, we investigated the performances of the network-based and the stand-alone EW systems on the central Italy sequence, playing back accelerometric data into the systems as they were recorded in real time. We found that the ground-shaking intensity was well predicted by both systems. Within 60 km from the event epicenter, the success rate of both EEWSs ranges between 85% and 90% for the main event of the sequence and is ~80% when considering all the events with magnitude larger than M_w 5.0 in the whole epicentral distance

range (< 130 km). Some missed alerts correspond to sites located within the BZ for which the radius on average is 20 km. The size of the BZ is significantly smaller than the size of the region where damages were reported for the M_w 6.5 earthquake (radius of about 40 km). The lead time for the regional system increases from 5 s at 30 km to 15 s at 55 km, allowing to trigger automatic security actions. These values halve for the on-site system, making this latter less effective for the area.

With this study, we show that an operational EEWS in central Italy might effectively contribute to mitigate the seismic risk during an earthquake and enhance postevent resiliency, provided that the delay due to telemetry and data packeting is significantly reduced.

DATA AND RESOURCES

Accelerograms used in this study were collected from the Italian Accelerometric Archive (ITACA) 2.0 (Pacor *et al.*, 2011) at http://itaca.mi.ingv.it (last accessed August 2017). Analysis and plots were made using MATLAB (https://it.mathworks.com/, last accessed August 2017). The Istituto Nazionale di Geofisica e Vulcanologia [INGV] catalog is available at http://cnt.rm.ingv.it (last accessed August 2017). PRESTo is a free and open-source platform, available at www.prestoews.org (last accessed October 2017). For the instrumental intensities estimated by the INGV, see http://shakemap.rm.ingv.it/shake/8863681/intensity.html (last accessed July 2017). For INGV network, see http://cnt.rm.ingv.it/instruments/network/IV (last accessed September 2017); for Engineering Strong Motion (ESM) database, see http://esm.mi.ingv.it/ (last accessed July 2017).

ACKNOWLEDGMENTS

The authors are grateful to Associate Editor Brendan Crowell and two anonymous reviewers that helped in improving the article. Real-time testing of the regional earthquake early warning system (EEWS) at the Near-Fault Observatory TABOO was organized in the framework of the EPOS-IP project. EPOS-IP has received funding from the European Union's HORIZON 2020 with Project ID 676564.

REFERENCES

Abrahamson, N. A., and J. J. Bommer (2005). Probability and uncertainty in seismic hazard analysis, *Earthq. Spectra* **21,** no. 2, 603–607.

Akkar, S., and J. J. Bommer (2007). Empirical prediction equations for peak ground velocity derived from strong-motion records from Europe and the Middle East, *Bull. Seismol. Soc. Am.* **97,** no. 2, 511–530.

Allen, R. M., and H. Kanamori (2003). The potential for earthquake early warning in southern California, *Science* **300,** 786–789, doi: 10.1126/science.1080912.

Arcoraci, L., F. Bernardini, R. Camassi, C. Castellano, S. Del Mese, E. Ercolani, A. Fodarella, L. Graziani, M. Locati, A. Maramai, *et al.* (2016). QUEST—Rilievo macrosismico per i terremoti nell'Italia central, *Aggiornamento dopo le scosse del 26 e 30 ottobre 2016. INGV Technical Report*, %%http://quest.ingv.it/images/rilievimacrosismici/QUEST_report%2018%20gennaio_17ErrCorr.pdf (last accessed July 2017) (in Italian).

Böse, M., T. H. Heaton, and E. Hauksson (2012). Real-time finite fault rupture detector (FinDer) for large earthquakes, *Geophys. J. Int.* **191,** no. 2, 803–812.

Caruso, A., S. Colombelli, L. Elia, M. Picozzi, and A. Zollo (2017). An on-site alert level early warning system for Italy, *J. Geophys. Res.* **122,** doi: 10.1002/2016JB013403.

Chiaraluce, L., R. Di Stefano, E. Tinti, L. Scognamiglio, M. Michele, E. Casarotti, M. Cattaneo, P. De Gori, C. Chiarabba, G. Monachesi, *et al.* (2017). The 2016 central Italy seismic sequence: A first look at the mainshocks, aftershocks, and source models, *Seismol. Res. Lett.* **88,** no. 3, doi: 10.1785/0220160221.

Colombelli, S., R. M. Allen, and A. Zollo (2013). Application of real-time GPS to earthquake early warning in subduction and strike-slip environments, *J. Geophys. Res.* **118,** no. 7, 3448–3461.

Colombelli, S., O. Amoroso, A. Zollo, and H. Kanamori (2012). Test of a threshold-based earthquake early warning using Japanese data, *Bull. Seismol. Soc. Am.* **102,** 1266–1275, doi: 10.1785/0120110149.

Colombelli, S., A. Caruso, A. Zollo, G. Festa, and H. Kanamori (2015). A P wave-based, on-site method for earthquake early warning, *Geophys. Res. Lett.* **42,** 1390–1398, doi: 10.1002/2014GL063002.

Colombelli, S., A. Zollo, G. Festa, and H. Kanamori (2012). Early magnitude and potential damage zone estimates for the great M_w 9 Tohoku-Oki earthquake, *Geophys. Res. Lett.* **39,** no. 22, L22306, doi: 10.1029/2012GL053923.

Colombelli, S., A. Zollo, G. Festa, and M. Picozzi (2014). Evidence for a difference in rupture initiation between small and large earthquakes, *Nature Commun.* **5,** 3958, doi: 10.1038/ncomms4958.

Emergeo W.G.Pucci, S., P. M. De Martini, R. Civico, R. Nappi, T. Ricci, F. Villani, C. A. Brunori, M. Caciagli, V. Sapia, *et al.* (2016). Coseismic effects of the 2016 Amatrice seismic sequence: First geological results, *Ann. Geophys.* **59,** doi: 10.4401/ag-7195.

Faenza, L., and A. Michelini (2010). Regression analysis of MCS intensity and ground motion parameters in Italy and its application in ShakeMap, *Geophys. J. Int.* **180,** 1138–1152, doi: 10.1111/j.1365-246X.2009.04467.x.

Festa, G., A. Zollo, and M. Lancieri (2008). Earthquake magnitude estimation from early radiated energy, *Geophys. Res. Lett.* **35,** L22307, doi: 10.1029/2008GL035576.

Iannaccone, G., A. Zollo, L. Elia, V. Convertito, C. Satriano, C. Martino, G. Festa, M. Lancieri, A. Bobbio, T. A. Stabile, *et al.* (2010). A prototype system for earthquake early-warning and alert management in southern Italy, *Bull. Earthq. Eng.* **8,** 1105–1129, doi: 10.1007/s10518-009-9131-8.

Iervolino, I., G. Baltzopoulos, and E. Chioccarelli (2016). Preliminary engineering analysis of the August 24th 2016, M_L 6.0 central Italy earthquake records, *Ann. Geophys.* **59,** doi: 10.4401/ag-7182.

Kanamori, H. (2005). Real-time seismology and earthquake damage mitigation, *Annu. Rev. Earth Planet. Sci.* **33,** 195–214, doi: 10.1146/annurev.earth.33.092203.122626.

Lancieri, M., and A. Zollo (2008). Bayesian approach to the real-time estimation of magnitude from the early P and S wave displacement peaks, *J. Geophys. Res.* **113,** no. B12302, doi: 10.1029/2007JB005386.

Liu, C., Y. Zheng, Z. Xie, and X. Xiong (2017). Rupture features of the 2016 M_w 6.2 Norcia earthquake and its possible relationship with strong seismic hazards, *Geophys. Res. Lett.* **44,** 1320–1328, doi: 10.1002/2016GL071958.

Livio, F. A., A. M. Michetti, E. Vittori, L. Gregory, L. Wedmore, L. Piccardi, E. Tondi, G. Roberts, and Central Italy Earthquake W. G., A. M. Blumetti, *et al.* (2016). Surface faulting during the August 24, 2016, central Italy earthquake (M_w 6.0): Preliminary results, *Ann. Geophys.* **59,** doi: 10.4401/ag-7197.

Lomax, A., C. Satriano, and M. Vassallo (2012). Automatic picker developments and optimization: FilterPicker—A robust, broadband picker for real-time seismic monitoring and earthquake early warning, *Seismol. Res Lett.* **83,** no. 3, 531–540, doi: 10.1785/gssrl.83.3.531.

Luzi, L., R. Puglia, E. Russo, M. D'Amico, C. Felicetta, F. Pacor, G. Lanzano, U. Çeken, J. Clinton, G. Costa, *et al.* (2016). The engineering

strong-motion database: A platform to access pan-European accelerometric data, *Seismol. Res. Lett.* **87,** no. 4, 987–997, doi: 10.1785/0220150278.

Pacor, F., R. Paolucci, G. Ameri, M. Massa, and R. Puglia (2011). Italian strong motion records in ITACA: Overview and record processing, *Bull. Earthq. Eng.* **9,** no. 6, 1741–1759, doi: 10.1007/s10518-011-9295-x.

Picozzi, M., D. Bindi, P. Brondi, D. Di Giacomo, S. Parolai, and A. Zollo (2017). Rapid determination of *P*-wave-based energy magnitude: Insights on source parameter scaling of the 2016 central Italy earthquake sequence, *Geophys. Res. Lett.* **44,** doi: 10.1002/2017GL073228.

Picozzi, M., A. Zollo, P. Brondi, S. Colombelli, L. Elia, and C. Martino (2015). Exploring the feasibility of a nationwide earthquake early warning system in Italy, *J. Geophys. Res.* **120,** 2446–2465, doi: 10.1002/2014JB011669.

Pucci, S., P. M. De Martini, R. Civico, F. Villani, R. Nappi, T. Ricci, R. Azzaro, C. A. Brunori, M. Caciagli, F. R. Cinti, *et al.* (2017). Coseismic ruptures of the 24 August 2016, M_w 6.0 Amatrice earthquake (central Italy), *Geophys. Res. Lett.* **44,** no. 5, 2138–2147, doi: 10.1002/2016GL071859.

Satriano, C., L. Elia, C. Martino, M. Lancieri, A. Zollo, and G. Iannaccone (2011). PRESTo, the earthquake early warning system for southern Italy: Concepts, capabilities and future perspectives, *Soil Dynam. Earthq. Eng.* **31,** no. 2, 137–153, doi: 10.1016/j.soildyn.2010.06.008.

Satriano, C., A. Lomax, and A. Zollo (2008). Real-time evolutionary earthquake location for seismic early warning, *Bull. Seismol. Soc. Am.* **98,** no. 3, 1482–1494, doi: 10.1785/0120060159.

Satriano, C., Y. M. Wu, A. Zollo, and H. Kanamori (2010). Earthquake early warning: Concepts, methods and physical grounds, *Soil Dynam. Earthq. Eng.* **31,** no. 2, 106–108, doi: 10.1016/j.soildyn.2010.07.007.

Sieberg, A. (1930). Geologie der Erdbeben, *Handbuch der Geophysik* **2,** no. 4, 550–555 (in German).

Tinti, E., L. Scognamiglio, A. Michelini, and M. Cocco (2016). Slip heterogeneity and directivity of the M_L 6.0, 2016, Amatrice earthquake estimated with rapid finite-fault inversion, *Geophys. Res. Lett.* **43,** 10,745–10,752, doi: 10.1002/2016GL071263.

Wu, Y. M., and H. Kanamori (2008). Development of an earthquake early warning system using real-time strong motion signals, *Sensors* **8,** no. 1, 1–9.

Yamada, M., and T. H. Heaton (2008). Real-time estimation of fault rupture extent using envelopes of acceleration, *Bull. Seismol. Soc. Am.* **98,** no. 2, 607–619.

Zollo, A., O. Amoroso, M. Lancieri, Y. M. Wu, and H. Kanamori (2010). A threshold-based earthquake early warning using dense accelerometer networks, *Geophys. J. Int.* **183,** 963–974, doi: 10.1111/j.1365-246X.2010.04765.x.

Zollo, A., S. Colombelli, A. Caruso, L. Elia, P. Brondi, A. Emolo, G. Festa, C. Martino, and M. Picozzi (2017). QuakeUp: An advanced tool for a network-based earthquake early warning system, *Geophys. Res. Abstr.* **19,** Abstract EGU 2017–14033.

Zollo, A., M. Lancieri, and S. B. Nielsen (2006). Earthquake magnitude estimation from peak amplitudes of very early seismic signals on strong motion, *Geophys. Res. Lett.* **33,** L23312, doi: 10.1029/2006GL027795.

Gaetano Festa
Matteo Picozzi
Alessandro Caruso
Simona Colombelli
Luca Elia
Mariano Supino
Aldo Zollo
Dipartimento di Fisica Ettore Pancini
Università di Napoli Federico II
Complesso Univ. Monte S. Angelo, via Cinthia
80126 Naples, Italy
gaetano.festa@unina.it

Marco Cattaneo
Simone Marzorati
Istituto Nazionale di Geofisica e Vulcanologia
Centro Pastorale "Stella Maris"
Via di Colle Ameno, 5
60126 Torette di Ancona, Italy

Lauro Chiaraluce
Istituto Nazionale di Geofisica e Vulcanologia
Via di Vigna Murata, 605
00143 Rome, Italy

Claudio Martino
Istituto Nazionale di Geofisica e Vulcanologia
Via Diocleziano, 328
80125 Naples, Italy

Published Online 22 November 2017